ADAPTATION IN THE QUINCUNX WAVELET FILTER BANK WITH APPLICATIONS IN IMAGE DENOISING

Miroslav Vrankic[1] *and Damir Sersic*[2]

[1]Faculty of Engineering, University of Rijeka
Vukovarska 58, HR-51000 Rijeka, CROATIA
[2]Faculty of Electrical Engineering and Computing, University of Zagreb
Unska 3, HR-10000 Zagreb, CROATIA
e-mail: Miroslav.Vrankic@RITEH.hr, Damir.Sersic@FER.hr

ABSTRACT

In this paper, we present the realization of an adaptive shift invariant wavelet transform defined on the quincunx grid. The wavelet transform relies on the lifting scheme which enables us to easily introduce the adaptation by splitting the predict stage into two parts. The first part of the predict stage is fixed and guarantees the number of vanishing moments of the wavelet filter bank while the second part can adapt to the local properties of the analyzed image. In this paper, we explore the robustness of the generalized least squares adaptation algorithm to the noise present in the analyzed image. The denoising results obtained with the nonseparable adaptive wavelet transform have been compared with results obtained with both separable and nonseparable fixed wavelet transforms. Also, the empirical Wiener filtering in the wavelet domain has been used in order to further improve the denoising results.

1 INTRODUCTION

In the field of image denoising, wavelets have been established as a very useful and effective tool. By using the wavelet transform, smooth regions of the image can be approximated very well with coarse approximation wavelet coefficients while most of the detail wavelet coefficients are zero or close to zero. On the other hand, edges (which contain most important information) as sharp transitions in the image are represented with high-valued detail coefficients. These properties of the wavelet transform guarantee the effectiveness of the image denoising procedure called wavelet shrinkage [1, 2].

When using the wavelet shrinkage to remove noise from the analyzed image, wavelet coefficients of the noisy image smaller than a given threshold are set to zero and the coefficients above the threshold are either left unchanged (hard thresholding) or reduced by the value of the threshold (soft thresholding). The higher the threshold, the more wavelet detail coefficients are being set to zero and the reconstructed image looks smoother. The good threshold is one that removes most of the noisy detail coefficients while still not oversmoothing the analyzed image, i.e. retaining the detail coefficients corresponding to the edges in the image.

The basic motivation of our research was to improve the wavelet transform by making it locally adaptive to the properties of the analyzed image. Such an improved wavelet transform would approximate better important features of the image and the detail wavelet coefficients would remain dominated with the noise. Wavelet shrinkage based on such an improved wavelet transform is expected to give better denoising results.

We have used the lifting scheme [3] in order to create an adaptive wavelet filter bank. Since the lifting scheme automatically guarantees perfect reconstruction of the resulting filter bank, it is very straightforward to introduce the adaptivity by simply making some of its basic building blocks adaptive.

A number of adaptive wavelet transforms based on the lifting scheme have been proposed in the literature. In [4], the lifting scheme with the adaptive prediction step has been used to create an adaptive filter bank structure. Unfortunately, important properties of the wavelet transform have been lost because of the fully adaptive prediction step.
Claypoole et al [5] have proposed locally adaptive wavelet transform for image coding based on the lifting scheme where the order of the prediction filter is being changed in order to avoid prediction across the discontinuities. In the smooth parts of the image higher order prediction filters are being used (resulting in wavelets with more zero moments), while near the edges lower order prediction filters are being used.
In [6] the update step in the lifting scheme has been made adaptive based on the local gradient information. The adaptation algorithm can be perfectly reproduced on the reconstruction side so that no additional bookkeeping is required.

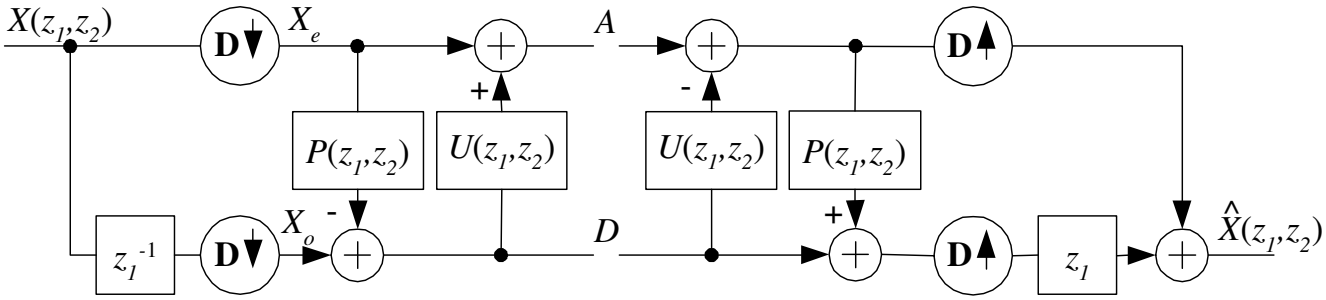

Figure 1: The two-channel analysis and synthesis filter banks based on the lifting scheme. Two-dimensional downsampling and upsampling is defined with the dilation matrix **D**.

As a starting point, we have used quincunx interpolating filter bank designed by Kovacevic and Sweldens [7] based on the lifting scheme. It results in the biorthogonal wavelet transform defined on the quincunx grid.
The quincunx sampling was chosen in order to obtain different orientational properties of the underlying wavelet decomposition. Such a nonseparable wavelet decomposition, contrary to the wavelets defined on the separable grid, is less biased in horizontal and vertical directions. Also, since the filter bank based on quincunx sampling consists of only two channels (compared to the four channels of the separable filter bank), it is much simpler and straightforward to introduce the adaptation.

2 ADAPTIVE LIFTING SCHEME

2.1 The Lifting Scheme

The lifting scheme shown in Figure 1 is built using three basic building blocks: split, predict and update. The first step is a polyphase decomposition, i.e. an image is being split into a number of phases (subimages).

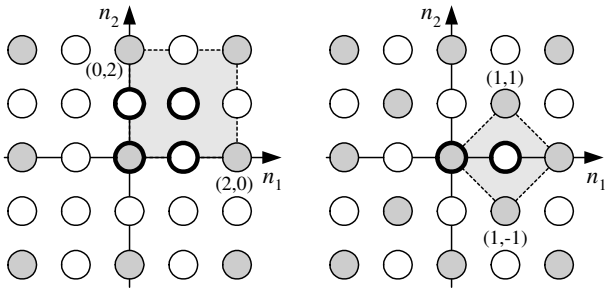

Figure 2: The two sampling schemes: separable (left) and quincunx (right). Each sampling lattice type is defined with its unit cell (area marked gray). Samples belonging to the unit cell are bolded. Each sampling scheme splits an image into as many phases (cosets) as there are samples in its unit cell.

If the separable sampling is applied we get four phases (Figure 2). If the quincunx sampling is applied, the image is being split into two phases (Figure 2 right).
For the case of only two phases, the predict filter P predicts values of pixels in the second phase based on the pixels from the first phase (Figure 3). The detail coefficients are simply calculated as a prediction error.

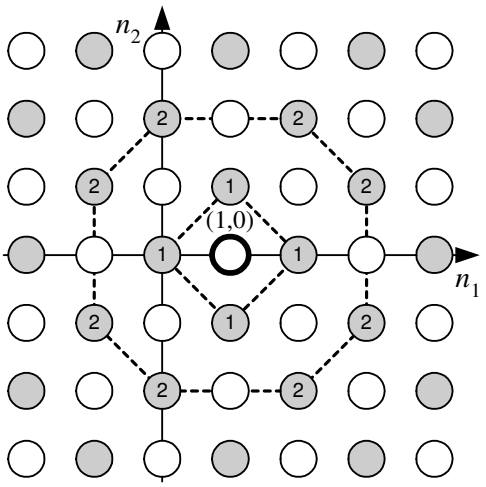

Figure 3: White circle marked bold belongs to the second quincunx coset. Its value is being predicted based on a number of nearest samples from the first coset. If the prediction filter P_2 of order two is being used, the prediction is based on the four samples marked with 1. If the prediction filter P_4 of order four is being used, the prediction is based on the twelve samples marked with 1 and 2.

The update filter U updates the value of the average wavelet coefficients based on the values of the previously obtained detail coefficients.
The synthesis filter bank is built by simply inverting the order and signs of the predict and update steps and joining the two phases together into the reconstructed image.

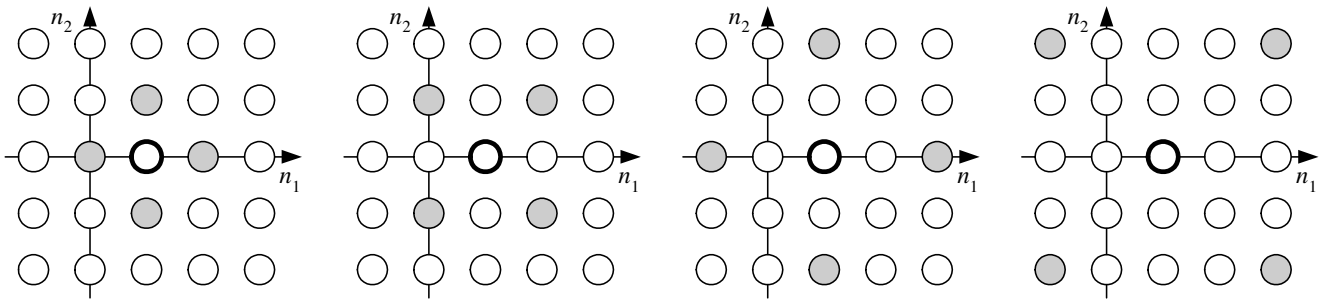

Figure 4: Gray circles mark supports of the quincunx-upsampled copies of the P_2 filter. From left to right: the P_2 filter has been upsampled on the quincunx grid once, twice, three times, and four times. These copies of the P_2 filter correspond to the predictors in the undecimated filter bank at decomposition levels one, two, three and four respectively. It can be seen that the prediction of the white sample marked bold is based on the four gray samples that are spread more for higher decomposition levels.

2.2 Quincunx Interpolating Filter Bank

In [7], Kovacevic and Sweldens propose the so-called Neville interpolating filters for various sampling grids as building blocks for the lifting scheme. For the quincunx case, they give the simplest prediction filter:

$$P_2(z_1, z_2) = \frac{1}{4}(1 + z_1^{-1} + z_2^{-1} + z_1^{-1}z_2^{-1}). \qquad (1)$$

It is the second order prediction filter which can perfectly predict values of polynomials of degree smaller than two. The fourth order prediction filter has wider support:

$$\begin{aligned} P_4(z_1, z_2) = &\frac{10}{32}(1 + z_1^{-1} + z_2^{-1} + z_1^{-1}z_2^{-1}) \\ &-\frac{1}{32}(z_1^{-2} + z_2^{-2} + z_1^{-2}z_2^{-1} + z_1^{-1}z_2^{-2} \\ &+z_1 + z_2 + z_1z_2^{-1} + z_1^{-1}z_2). \end{aligned} \qquad (2)$$

Supports of the P_2 and P_4 filters in the domain of the undecimated image are shown in Figure 3. Finally, the update filter is obtained as half the adjoint of the corresponding predict filter.

$$U_2(z_1, z_2) = \frac{1}{2}P_2^*(z_1, z_2) = \frac{1}{8}(1 + z_1 + z_2 + z_1z_2). \quad (3)$$

Using P_2 and U_2 filters results in a biorthogonal wavelet filter bank with two vanishing moments of a primal wavelet, and two vanishing moments of a dual wavelet. Using the P_4 prediction filter instead, results in increasing the number of vanishing moments of a dual wavelet to four.

2.2.1 Undecimated Filter Bank

It has been shown that significantly improved image denoising results are obtained when using the undecimated wavelet transform [8]. For the purpose of image denoising we have used undecimated version of the quincunx wavelet filter bank. In such a structure decimation operators are removed, and in every level of the iterated filter bank structure the appropriately quincunx-upsampled P and U filters are used. For example, in the N-th decomposition level, N-times quincunx-upsampled versions of P and U filters are used. Knowing that the dilation matrix which defines quincunx upsampling is $\mathbf{D} = \begin{bmatrix} 1 & 1 \\ -1 & 1 \end{bmatrix}$ and writing $\mathbf{z} = \begin{bmatrix} z_1 \\ z_2 \end{bmatrix}$, the N-times quincunx-upsampled filter P equals $P(\mathbf{z}^{\mathbf{D}^N})$. For example, in the first level of the undecimated filter bank structure, the second order prediction filter becomes:

$$\begin{aligned} P_2(\mathbf{z}^{\mathbf{D}}) =& P_2(z_1z_2^{-1}, z_1z_2) \\ =& \frac{1}{4}(1 + z_1^{-1}z_2 + z_1^{-1}z_2^{-1} + z_1^{-2}). \end{aligned} \qquad (4)$$

Examples of the support of the upsampled P_2 filter are shown in Figure 4.

2.3 Adaptive Prediction Step

As previously reported in [9], we propose to split the prediction branch into two parts in order to introduce the adaptivity (see Figure 5). The first prediction branch contains the second order prediction filter P_2 which is fixed. The second branch contains the filter $P_{42} = P_4 - P_2$, whose output is multiplied with the p parameter which can be changed according to the local image properties.

Although the overall prediction structure is adaptive, the polynomial reconstruction property of the wavelet transform (number of vanishing moments) is ensured by the fixed prediction branch. Since the P_2 filter is used in the fixed prediction branch, the two vanishing moments of a dual (analysis) wavelet are guaranteed no matter what values the adaptive parameter p may take. It further means that the primal (synthesis) scaling function is able to perfectly reproduce polynomials of a degree lower than two.

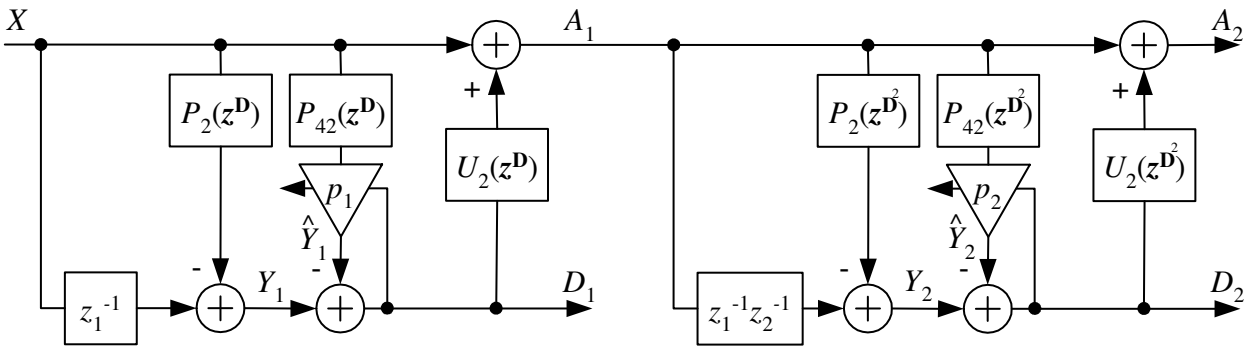

Figure 5: The first two decomposition levels of the adaptive filter bank. The filter in the adaptive prediction branch $P_{42} = P_4 - P_2$. In each decomposition level i, for each pixel (j,k), the $p_i(j,k)$ parameter has been calculated as the LS solution that minimizes weighted squared norm $\|\mathbf{d}_i(j,k)\|_w^2 = \|\mathbf{y}_i(j,k) - \hat{\mathbf{y}}_i(j,k)\|_w^2$ based on a 3x3 pixels wide neighborhood of (j,k).

The reason for having the two dual vanishing moments guaranteed although the overall prediction structure is adaptive lies in the fact that the P_{42} filter always has the zero output for the inputs that are polynomials of order lower than two. So, no matter what values the adaptive parameter p may take, the adaptive structure pP_{42} will not have any effect for polynomials of order lower than two.

2.3.1 Generalized Least Squares Adaptation

When using the lifting scheme, the wavelet detail coefficients are obtained as an error of predicting samples from the second phase based on a number of samples from the first image phase. We have chosen to adapt the p parameter in order to minimize the squared prediction error which actually leads to minimizing the energy of the detail coefficients. The least squares (LS) solution for the $p_i(j,k)$ parameter in the i-th decomposition level has been calculated based on a window 3x3 pixels big that symmetrically surrounds the point (j,k).

Contrary to the plain windowed LS algorithm used in [9], we have used generalized LS windowed adaptation algorithm for the purpose of image denoising. Necessity of using the generalized LS approach comes from the fact that the additive zero-mean white Gaussian noise present in the image has been colored when passing through the filter bank structure and the signal $\mathbf{y}_i$ (Figure 5) contains its high-pass filtered version. The generalized LS solution for (j,k)-th pixel in the i-th decomposition level is obtained as

$$p_{ijk} = (\mathbf{A}_{ijk}^{\mathrm{T}}\mathbf{R}_i^{-1}\mathbf{A}_{ijk})^{-1}\mathbf{A}_{ijk}^{\mathrm{T}}\mathbf{R}_i^{-1}\mathbf{y}_{ijk}. \qquad (5)$$

where $\mathbf{R}_i$ is the the covariance matrix of the colored noise present in the high-pass signal $\mathbf{y}_i$. For simplicity, we have used $\mathbf{R}_i$ that has been calculated for the case of the fixed filter bank structure with only P_2 and U_2 filters. The vector $\mathbf{y}_{ijk} = \mathbf{y}_i(j,k)$ contains 9 entries corresponding to 9 samples of the $\mathbf{y}_i$ signal from the 3x3 window that surrounds the point (j,k). Since the unknown $p_i(j,k)$ is just a scalar, the matrix $\mathbf{A}_{ijk} = \mathbf{A}_i(j,k)$ contains only one column with 9 corresponding values of the output of the P_{42} filter.

3 IMAGE DENOISING

By using this adaptive approach, the important features of the image are expected to be mostly stored in the locally adapted wavelet functions, defined by the values of p parameters, while the detail coefficients are expected to remain dominated with the noise.

We will demonstrate such a behavior by a simple example in order to give motivation for more realistic applications of this approach. Gaussian noise has been added to the two-dimensional sine wave shown in Figure 6(a). The resulting noisy image is shown in Figure 6(b). First, we have used simple wavelet shrinkage based on the fixed quincunx wavelets (will be explained in more detail in section 4). Using soft thresholding, we obtained the result shown in Figure 6(c). After that, we have calculated the p parameters of the clean image based on the LS criterion. It is important to note that in this case the adaptation was perfect - all detail coefficients have been set to zero. We have used these p parameters for the decomposition of the noisy image. It is obvious that the obtained nonzero detail wavelet coefficients correspond to the noise present in the image. Setting all the detail coefficients in all decomposition levels to zero and reconstructing the image we get the result shown in 6(d) that is almost the same as the original image.
Of course, in real applications, the clean image is unknown so we do not have these "oracle" p parameters but having the adaptation algorithm that is robust enough to the presence of the noise should give results closed to these.

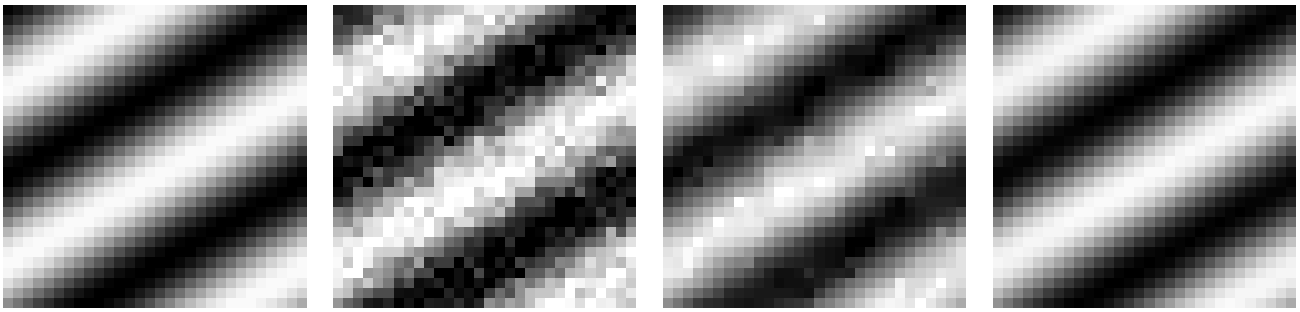

(a) Original image X (b) Noisy image Xn (c) Quincunx wavelet shrinkage of Xn (d) Oracle quincunx wavelet shrinkage of Xn

Figure 6: Denoising results of a two-dimensional sine wave image (a). Gaussian noise with zero mean and standard deviation $\sigma = 20$ has been added to the two-dimensional sine wave with amplitude 100 (b). Quincunx wavelet shrinkage (c) has been performed using soft thresholding with the normalized threshold $N = 0.75$ (optimal value of N regarding PSNR).

3.1 Empirical Wiener Filtering in the Wavelet Domain

Finally, we have experimented by combining our adaptive wavelets approach with the empirical wavelet domain Wiener filtering. The basic idea is to perform wavelet shrinkage based on the adaptive wavelet transform and then reuse that result as a pilot estimate for the Wiener-like thresholding in the separable wavelet domain. This two-stage empirical Wiener filtering scenario as proposed in [10] is shown in Figure 7. It can

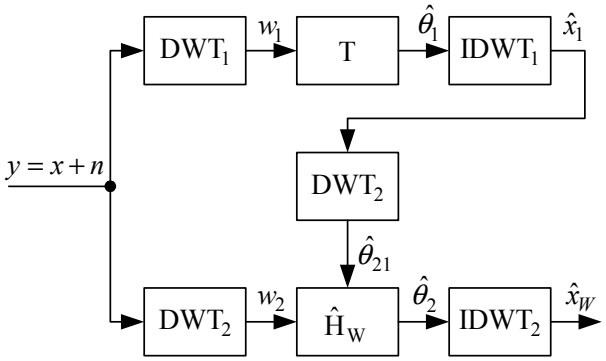

Figure 7: Empirical Wiener filtering in the wavelet domain.

be seen that two transforms are used. In the domain of the primary transform (DWT1) the wavelet shrinkage is performed in order to obtain a pilot estimate of the clean image. Then, the secondary wavelet transform (DWT2) is used to spread the primary wavelet-domain thresholded coefficients and to reevaluate them by weighting the noisy wavelet coefficients. This weighting is obtained with the empirical Wiener filter $\hat{H}_W$ as:

$$\hat{\theta}_2(i,j) = \frac{\hat{\theta}^2_{21}(i,j)}{\hat{\theta}^2_{21}(i,j) + \hat{\sigma}^2} w_2(i,j) = \hat{H}_W(i,j) w_2(i,j), \tag{6}$$

where w denotes the wavelet coefficients of the noisy image y and $\hat{\sigma}$ is the estimated noise deviation [11]. We have used separable wavelets for the secondary wavelet transform in order to increase the mismatch between the two transforms and to obtain a more reliable estimate of the clean image.

4 RESULTS AND CONCLUSIONS

For the purpose of wavelet shrinkage we have used eight-level adaptive wavelet decomposition based on the structure as shown in figure 5. In Figures 8 and 9 this method is denoted as Qa. Since the employed filter bank is biorthogonal, different threshold weights have been applied for each decomposition level. The threshold value is obtained as a weighted multiple of the noise deviation: $T_{\mathrm{Qa}} = N\sigma W$. The weights have been obtained empirically and for levels from 1 to 8 (finest to coarsest) they are: $W = \{2.5\ 1.5\ 0.9\ 0.8\ 0.7\ 0.6\ 0.5\ 0.4\}$. We have experimented with both soft and hard thresholding.

Also, wavelet shrinkage has been performed using the calculated p parameters of the clean image based on the LS criterion in order to show how good the Qa method could perform. It will be denoted with Qo, as wavelet shrinkage based on oracle adapted quincunx wavelets.

These results will be compared with the ones obtained by using fixed separable (S) and quincunx (Q) wavelets. First, we have used separable Daubechies wavelets of order two (*db2*). To obtain comparable results with quincunx wavelets, we have used four-level wavelet decomposition and the threshold $T_{\mathrm{S}} = N\sigma$ has been tested for various values of N. Next, we have tested the performance of the fixed quincunx wavelets based on the P_2 and U_2 lifting steps.

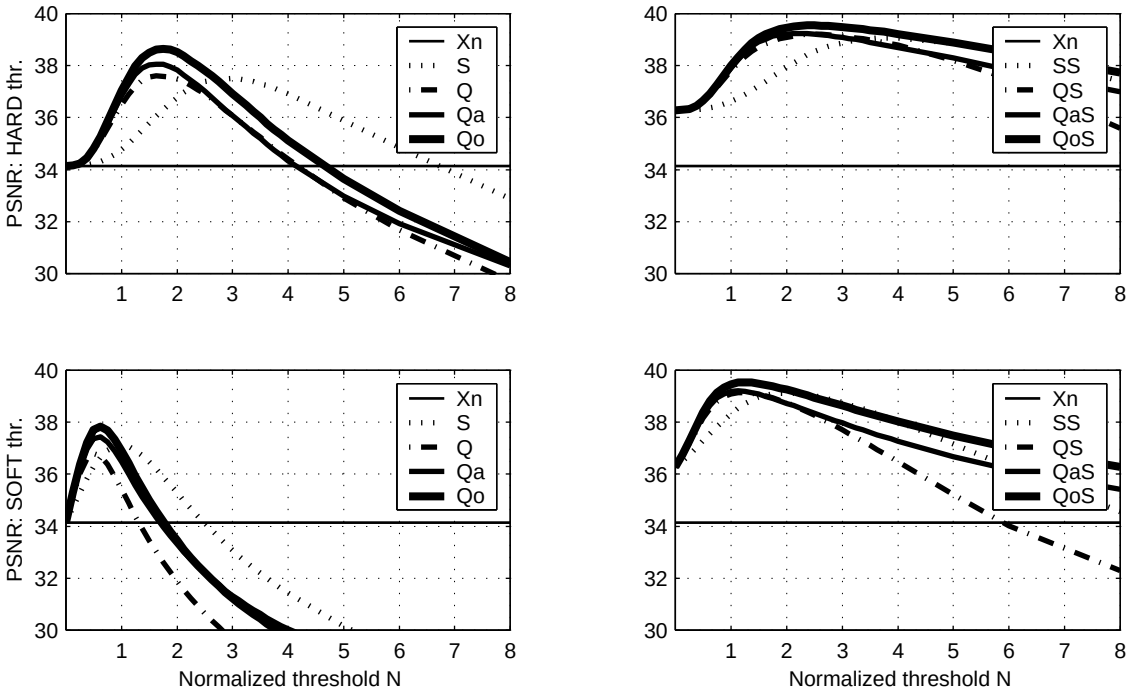

(a) $\sigma = 5$

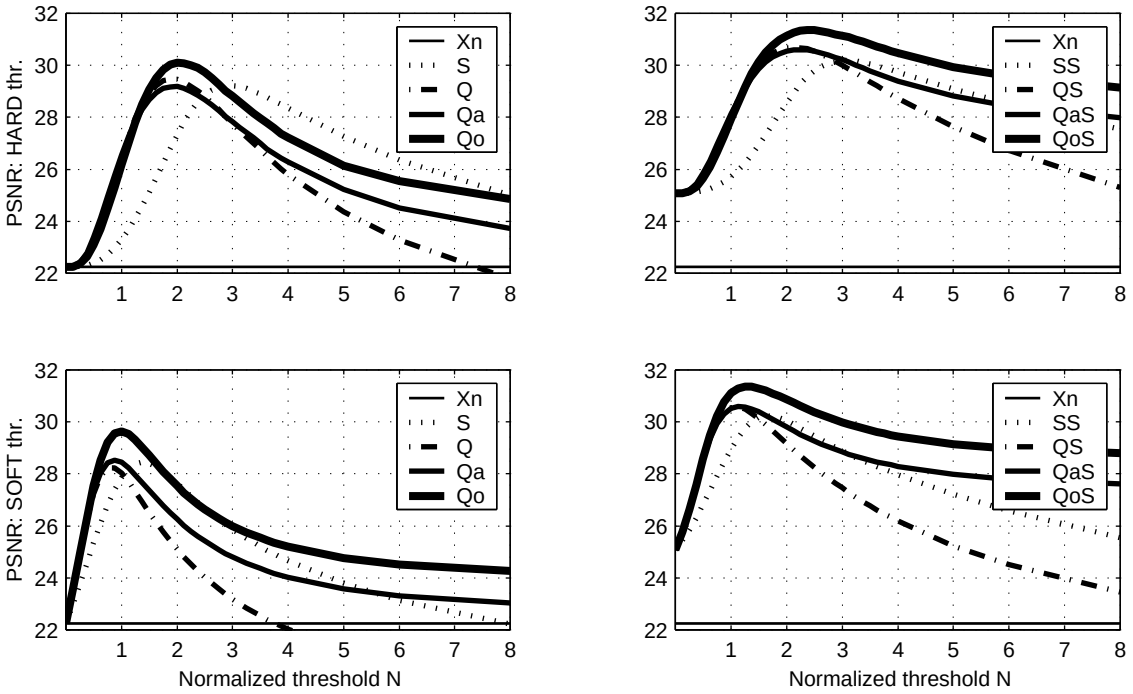

(b) $\sigma = 20$

Figure 8: Denoising results in terms of peak signal to noise ratio (PSNR) for the Bike image with additive Gaussian noise with (a) $\sigma = 5$ and (b) $\sigma = 20$. Both hard thresholding (graphs in first rows) and soft thresholding (graphs in second rows) results are shown. PSNR values against normalized threshold N are shown in the first column for wavelet shrinkage based on different wavelet decompositions: S - separable wavelets, Q - quincunx wavelets, Qa - adaptive quincunx wavelets, Qo - oracle adapted quincunx wavelets. Second column gives denoising results of empirical wavelet domain Wiener filtering. The previous results obtained with S, Q, Qa and Qo are used as pilot estimates for the Wiener-like thresholding in the domain of the second separable wavelet transform. So, based on S, Q, Qa and Qo pilot estimates, the SS, QS, QaS and QoS respectively are obtained. Horizontal solid line represents the PSNR of the noisy image Xn.

In order to show how much can all these methods be further improved, we have applied empirical wavelet-domain Wiener filtering. The previously obtained denoised images have been used as pilot estimates and then the Wiener-like thresholding in the domain of the second separable wavelet transform has been performed. For the second wavelet transform, we have used symlet wavelets of order six (*sym6*). The Wiener filtering-based methods based on S, Q, Qa and Qo pilot estimates are denoted in the following figures as SS, QS, QaS and QoS respectively.

When comparing results from Figure 8 it can be seen that as the noise variance increases, the improvement of wavelet shrinkage based on oracle adapted quincunx wavelets over the wavelet shrinkage based on fixed wavelets increases. In Figure 8(b) it can be seen that as the threshold value increases, the image denoising performance of nonadaptive wavelet decompositions decreases faster than the performance of wavelet shrinkage methods based on adaptive wavelets. It proves that the adaptivity incorporated in the filter bank transferred a part of the important image information in the adapted wavelet functions defined by the values of the p parameters and the higher values of the threshold affects more the noise than the original image features.

Still, the gain when using adaptive wavelets is not as big as it might have been expected. Usually, the gain in terms of peak signal to noise ratio (PSNR) is not higher than 1.5 dB. As shown in the right columns of Figures 8(a) and 8(b), more significant improvement can be obtained by reusing the adaptive denoising results in the framework of empirical Wiener filtering.

Also, the quincunx adaptive wavelets (Qa) do not follow the improvement of oracle adaptive wavelets (Qo). In fact, it is quite opposite: the improvement of the Qa method over the wavelet shrinkage method based on fixed wavelets gets smaller as noise variance increases. It shows that the generalized LS approach is not able to cope adequately with the noise present in the image. The problem lies in the fact that generalized LS solution assumes that the matrix $\mathbf{A}_{ijk}$ of equation 5 is noiseless. In our case it is not the fact since the colored noise is also present at the output of the P_{42} filter. We expect the solution of this problem to be in the total least squares approach and errors-in-variables modelling.

The reason that the oracle adaptive wavelet decomposition does not show such a significant improvement as it was expected is that the adaptation algorithm performed on the clean real-world images does not manage to give a wavelet decomposition that perfectly models the real-world images. In other words, it doesn't manage to turn all the detail coefficients of the original clean image to zero. Our ongoing research is focused on solving this problem by changing the adaptive multiplier p with the adaptive filter with 2x2 coefficients which would be able to reflect better the directional properties of the original image.

5 References

[1] D. L. Donoho and I. M. Johnstone, "Ideal spatial adaptation by wavelet shrinkage," *Biometrika*, vol. 81, no. 3, pp. 425–455, 1994.

[2] D. L. Donoho and I. M. Johnstone, "Adapting to unknown smoothness by wavelet shrinkage," *Journal of the American Statistical Association*, vol. 90, pp. 1200–1224, 1995.

[3] W. Sweldens, "The lifting scheme: A custom-design construction of biorthogonal wavelets," *Appl. Comput. Harmon. Anal.*, vol. 3, no. 2, pp. 186–200, 1996.

[4] O. N. Gerek and A. E. Cetin, "Adaptive polyphase subband decomposition structures for image compression," *IEEE Trans. Image Processing*, vol. 9, pp. 1649–1659, 2000.

[5] W. S. R. L. Claypoole, G. Davis and R. D. Baraniuk, "Nonlinear wavelet transforms for image coding," vol. 1, pp. 662–667, 1997.

[6] G. Piella and H. J. A. M. Heijmans, "Adaptive lifting schemes with perfect reconstruction," *IEEE Trans. Signal Processing*, vol. 50, pp. 1620–1630, July 2002.

[7] J. Kovačević and W. Sweldens, "Wavelet families of increasing order in arbitrary dimensions," *IEEE Trans. Image Proc.*, vol. 9, pp. 480–496, March 2000.

[8] R. R. Coifman and D. Donoho, "Time-invariant wavelet de-noising," in *Wavelets and Statistics* (A. Antoniadis and G. Oppenheim, eds.), vol. 103 of *Lecture Notes in Statistics*, (New York), pp. 125–150, Springer-Verlag, 1995.

[9] M. Vrankić and D. Seršić, "Adaptation methods of 2-d nonseparable wavelet filter bank," in *Proc. of the Second International Workshop on Spectral Methods and Multirate Signal Processing*, (Toulouse, France), pp. 235–242, September 2002.

[10] Ghael and Baraniuk, "Improved wavelet denoising via empirical wiener filtering," in *SPIE*, 1995.

[11] I. M. Johnstone and B. W. Silverman, "Wavelet threshold estimators for data with correlated noise," *Journal of the Royal Statistical Society B*, vol. 59, no. 2, pp. 319–351, 1997.

(a) Noisy image Xn (b) S, with $T_{\mathrm{S}} = 30$ (c) Q, with $T_{\mathrm{Q}} = 20W$

(d) Qa, with $T_{\mathrm{Qa}} = 20W$ (e) SS, using pilot estimate S (f) QS, using pilot estimate Q

(g) Qo, with $T_{\mathrm{Qo}} = 20W$ (h) QaS, using pilot estimate Qa (i) QoS, using pilot estimate Qo

Figure 9: Denoising results in terms of PSNR for the Bike image with additive Gaussian noise with $\sigma = 20$. The pilot estimates S, Q, Qa and Qo have been obtained by using soft thresholding with different thresholds.